ACS OMEGA
Open Access

http://pubs.acs.org/journal/acsodf
Article

Highly Efficient Cauliflower-like Palladium-Loaded Porous MOF as a Robust Material for the Degradation of Organic Dyes

Rimi, Pardeep Kumar, Bhawna Uttam,* and Ravi Kumar*

Cite This: *ACS Omega* 2023, 8, 38895–38904

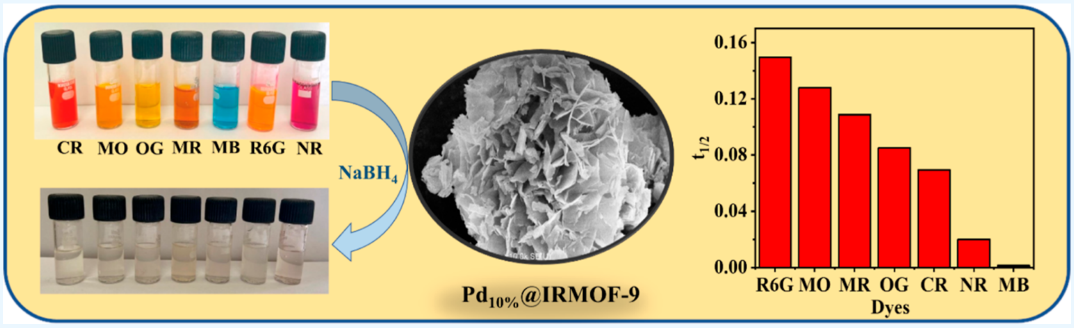

ABSTRACT: A series of porous MOF materials, viz., Pd_x@IRMOF-9 (x = 2, 5, and 10%) were synthesized by loading varying concentrations of Pd(II) on IRMOF-9. The synthesized MOF materials were characterized by ltravioletisible (UV–Vis) spectroscopy, Fourier transform Infrared (FT-IR) spectroscopy, powder X-ray diffraction (PXRD), Brunauer–Emmett–Teller (BET), and scanning electron microscopy (SEM) analyses. UV, FT-IR, and PXRD data of Pd(II)@IRMOF-9 were found to be in line with those of IRMOF-9, which suggests that the structure of the IRMOF-9 remained intact upon Pd(II) loading. Surface morphology of IRMOF-9 showed sheet-like structures, and upon incorporation of Pd(II) to IRMOF-9, porous cauliflower-shaped MOFs were obtained. The SEM area mapping of $Pd_{10\%}$@IRMOF-9 confirmed the homogeneous dispersion of Pd(II) on IRMOF-9. BET measurements suggested an increase in the surface area as well as pore size upon incorporation of Pd(II) on IRMOF-9. Due to high porosity and high petal density, $Pd_{10\%}$@IRMOF-9 demonstrated degradation of seven organic dyes, namely, orange G, methylene blue, methyl orange, congo red , methyl red, rhodamine 6G, and neutral red. It showed excellent results with >90% dye degradation efficiency in case of cationic, anionic as well as neutral dyes. Degradation of organic dyes followed the pseudo-first-order kinetics. Kinetic parameters, K_M and V_{max}, were calculated using the double reciprocal Lineweaver–Burk plot and were found to be 13.2 μM and 26.68 × 10^{-8} M min^{-1}, respectively. Recyclability studies of heterogeneous $Pd_{10\%}$@IRMOF-9 demonstrated the degradation of CR dye for five consecutive cycles without significant loss of its catalytic activity. Herein, a robust and efficient material for the degradation of organic dyes has been developed and demonstrated.

■ INTRODUCTION

Metal–organic frameworks (MOFs) are a class of crystalline three-dimensional highly porous materials synthesized from metal ions and polyfunctional ligands. MOFs have a high surface area, tunable coordination sites, and high thermal and chemical stability.[1,2] Due to these properties MOFs have been used in catalysis,[3−7] biomedicine,[8−12] electrochemical applications,[13] gas recovery and storage[14−16] as well as for the adsorption[17−20] and photodegradation[21−24] of various organic contaminants. Tunable coordination space and cavities of MOFs make them potential materials for the encapsulation of metal ions.[25] During past years, the interaction between the MOF support and the active metals has been extensively studied for catalytic reactions because of their enhanced catalytic properties that arise from this combination. Such kind of MOFs has been utilized in various types of organic transformations, such as synthesis of imines, benzoxazoles, catalytic hydrogenation, and coupling reactions.[26−30] However, some active-metal-loaded MOFs have also been effectively used for the degradation of organic contaminants, such as nitroaromatics and dyes.[31−33] In the present scenario, the removal of organic dye pollutants from water bodies is a bigger challenge. Organic dyes are widely used for various industrial applications such as textile and food manufacturing, and most of their residual waste is released into water. These dyes cause serious health problems to humans as well as aquatic animals due to their high chemical oxygen demand and carcinogenic

Received: May 2, 2023
Accepted: September 26, 2023
Published: October 13, 2023

https://doi.org/10.1021/acsomega.3c03014
ACS Omega 2023, 8, 38895–38904

Scheme 1. Schematic Illustration for the Synthesis of IRMOF-9 and $Pd_{x\%}$@IRMOF-9

$$\text{Zinc Nitrate hexahydrate} + \text{Biphenyl-4,4'-dicarboxylic acid} \xrightarrow[100°C,\ 18\ h]{DMF} \text{IRMOF-9} \xrightarrow[\text{Toluene, rt, 24 h}]{Pd(OAc)_2} Pd_{x\%}@\text{IRMOF-9}$$

where, x=2%, 5%, 10%

nature.[34−36] Several reports have been published for the reduction of dyes using noble metals (Pt, Pd, and Au) dispersed on a solid support, such as activated carbon,[37,38] polymeric materials,[39,40] and MOFs.[31−33,41] In this regard, MOFs have been demonstrated as efficient materials for the degradation of organic pollutants, and among them Zn-based MOFs have been extensively explored .[42] Yaghi and co-workers synthesized IRMOF-9, containing oxide-centered Zn_4O as a simple basic unit (SBU) and 4,4′-biphenyl dicarboxylate as an organic linker.[43] IRMOF-9 has been explored for the nitrogen adsorption,[44] CO_2 uptake, and in the field of sensing.[45] Literature reports based on IRMOF-9 suggest that utilization of IRMOF-9 in different fields is still in its infancy stage. Various modified analogues of IRMOF-9 have been synthesized and used as catalysts in various organic transformations.[46−48]

We herein report the synthesis of a series of heterogeneous, porous, and cauliflower-shaped Pd(II)-doped materials, i.e., $Pd_{2\%}$@IRMOF-9, $Pd_{5\%}$@IRMOF-9, and $Pd_{10\%}$@IRMOF-9 by loading of 2, 5, and 10% Pd(II) on IRMOF-9 using an impregnation technique. Out of these synthesized MOF materials, $Pd_{10\%}$@IRMOF-9 has been successfully investigated for the degradation of a variety of organic dyes.

■ EXPERIMENTAL SECTION

The chemicals used in this work were used as received without further purification. Biphenyl dicarboxylic acid and zinc nitrate hexahydrate were procured from TCI Chemicals. The solvents used in the reaction were of analytical grade, and Milli-Q water was used for the present study. All of the organic dyes were purchased from Sigma-Aldrich. Fourier Transform Infrared (FT-IR) and Ultraviolet−Visible (UV−vis) spectra were measured on a PerkinElmer spectrometer (UTAR Two) and a Shimadzu UV-3600i Plus UV−vis−NIR spectrophotometer, respectively. A quartz cuvette of 3 mL capacity and 1 cm path length was used for absorption studies. Scanning electron microscopy (SEM) images were taken on a JSM-7600 field electron gun-scanning electron microscope and a Hitachi SU8010 field emission scanning electron microscope. Inductively coupled plasma−mass spectrometry (ICP−MS) studies were done on an Agilent 7900 ICP−MS instrument. Nitrogen adsorption measurements were performed on a Quantachrome Autosorb iQ station 3 at 77 K. Approximately 30 mg of each MOF sample was added to a preweighed 9 mm sample cell. Both the samples were activated under vacuum at 200 °C for 2 h. The activated MOF samples were used for analysis for 1.5 h. Brunauer−Emmett−Teller (BET) surface areas and pore volumes were calculated by using Quantachrome ASiQwin software.

X-ray photoelectron spectroscopy (XPS) analysis was carried out on a Kratos Analytical instrument (AXIS Supra model). Powder X-ray diffraction (PXRD) studies were carried out on a Panalytical X'Pert Pro.

Synthetic Procedure of IRMOF-9. IRMOF-9 was synthesized by the reported procedure using some modifications.[44] To a solution of $Zn(NO_3)_2·6H_2O$ (180 mg, 0.605 mmol) in *N*,*N*-dimethyl formamide (DMF) (4 mL), 4,4′-biphenyldicarboxylic acid (BPDC) (30 mg, 0.124 mmol) was added. The resultant mixture was allowed to stir for 15 min at room temperature to form a homogeneous solution. The solution was placed in a preheated oven at 100 °C for 18 h. Colorless cubic crystals obtained after 18 h were thoroughly washed with fresh DMF three times. The resulting crystals were immersed in chloroform for 3 days. A white crystalline powder of IRMOF-9 was obtained. The as-synthesized IRMOF-9 was characterized by FTIR, UV−vis, BET, PXRD, and SEM.

Synthesis of Pd_x@IRMOF-9. A series of Pd_x@IRMOF-9 having different concentrations of Pd(II), viz., $Pd_{2\%}$@IRMOF-9, $Pd_{5\%}$@IRMOF-9, and $Pd_{10\%}$@IRMOF-9 were synthesized. For the preparation of $Pd_{10\%}$@IRMOF-9, to a solution of $Pd(OAc)_2$ (10 mg, 0.0445 mmol) in toluene (2 mL) was added IRMOF-9 (100 mg) in a 5 mL sample vial. The resultant heterogeneous solution was allowed to stir at room temperature for 24 h at 220 rpm. The resulting brown color solid was separated by centrifugation, followed by washing with acetone (three times), and dried under vacuum. Yield = 95 mg.

Using similar reaction conditions, $Pd_{2\%}$@IRMOF-9 and $Pd_{5\%}$@IRMOF-9 were prepared by taking 2 mg (0.0089 mmol) and 5 mg (0.02227 mmol) of $Pd(OAc)_2$, respectively. The synthesized $Pd_{2\%}$@IRMOF-9, $Pd_{5\%}$@IRMOF-9, and $Pd_{10\%}$@IRMOF-9 MOF materials were characterized by PXRD, FTIR, UV−Vis, and SEM analyses.

Sample Preparation for Microscopy. One mg of powdered MOF (IRMOF-9, $Pd_{2\%}$@IRMOF-9, $Pd_{5\%}$@IRMOF-9, and $Pd_{10\%}$@IRMOF-9) was suspended in 1 mL of ethanol and allowed to sonicate for 30 min. From the dispersed sample, 10 μL solution was drop-cast on a small piece of aluminum foil and dried. The dried samples were mounted on carbon tape (sample stub) to check the morphology of the samples.

Absorption Parameters of Organic Dyes. Reductive degradation studies of various organic dyes, such as Congo red (CR), Methyl orange (MO), Orange G (OG), Methylene blue (MB), Rhodamine 6G (R6G), Methyl red (MR), and Neutral red (NR), were carried out in water using $Pd_{10\%}$@IRMOF-9 in the presence of $NaBH_4$. The concentration of the stock solution of organic dyes prepared in water was 25 μM. The experiments were performed in a quartz cuvette by taking 2.7 mL of 25 μM dye and 250 μL of 0.01 M $NaBH_4$ in the case of all organic dyes. The concentration of stock solution of $Pd_{10\%}$@IRMOF-9 material used was 10 mg/mL, having a cuvette concentration of 0.083 mg/mL in the case of all the dyes. The kinetic studies were performed in the case of CR dye by varying the $Pd_{10\%}$@IRMOF-9 concentration (0.033, 0.083, 0.13, 0.18, 0.23, and 0.33 mg/mL) and keeping the dye concentration constant as 22.5 μM. The degradation of all the dyes was monitored by UV−Vis absorption spectra with respect to time.

Recyclability Studies. A recycling experiment was performed for the degradation of CR dye by using the $Pd_{10\%}$@IRMOF-9 material. The material was recovered for use in the next cycle by centrifugation, followed by washing with water and acetone. The recyclability experiments were carried

https://doi.org/10.1021/acsomega.3c03014
ACS Omega 2023, 8, 38895−38904

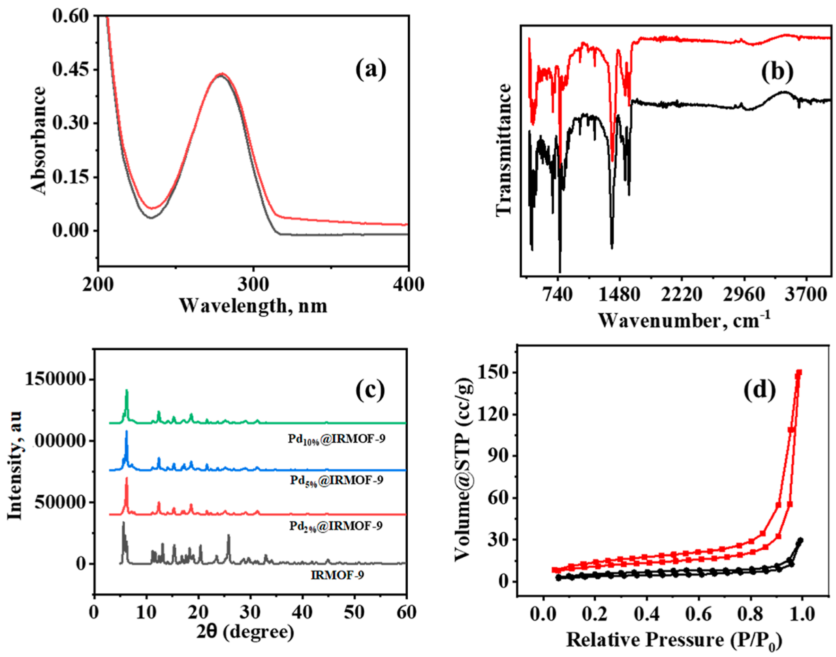

Figure 1. Graphs of IRMOF-9 and $Pd_{10\%}$IRMOF-9. (a) UV−vis spectra, (b) FTIR spectra, (c) PXRD patterns, and (d) nitrogen sorption isotherms of IRMOF-9 and $Pd_{10\%}$@IRMOF-9 at 77 K. Black and red colors correspond to data of IRMOF-9 and $Pd_{10\%}$IRMOF-9, respectively, in case of (a), (b), and (d).

out in a quartz cuvette by taking 2.7 mL of CR dye (25 μM), 250 μL of $NaBH_4$ (0.01 M), and 25 μL of recycled catalyst. The stock solution of the recycled catalyst used was 10 mg/mL.

RESULTS AND DISCUSSION

Synthetic Scheme of Pd@IRMOF-9. IRMOF-9 was synthesized by the procedure given above in the Experimental Section, and the Pd (II) was immobilized on IRMOF-9 *via* an impregnation technique that resulted in the formation of Pd_x@IRMOF-9, where *x* is 2, 5, and 10%, as shown in Scheme 1. IRMOF-9, $Pd_{2\%}$@IRMOF-9, $Pd_{5\%}$@IRMOF-9, and $Pd_{10\%}$@IRMOF-9 were characterized by various characterization techniques such as IR, UV, PXRD, and SEM analyses.

IRMOF-9 and $Pd_{10\%}$@IRMOF-9 show an absorbance peak at λ_{max} = 280 nm, as can be noticed from Figure 1a. FT-IR spectra of IRMOF-9 is similar to that reported in the literature.[44] The peak observed at 1660 cm^{-1} corresponds to the C═O stretching frequency of the BPDC ligand of IRMOF-9 (Figure 1b). PXRD analysis was performed for IRMOF-9, whose result is consistent with the reported literature data.[44] The PXRD data of $Pd_{2\%}$@IRMOF-9, $Pd_{5\%}$@IRMOF-9, and $Pd_{10\%}$@IRMOF-9 show that there is no apparent loss in the crystallinity of MOF after the immobilization of Pd(II) (Figure 1c). The percentage loading of Pd(II) estimated by ICP−MS was found to be ∼1.013% of Pd loaded in the case of $Pd_{10\%}$@IRMOF-9.

The BET measurements of $Pd_{10\%}$@IRMOF-9 revealed that doping with Pd(II) on IRMOF-9 results in a significant enhancement in the surface area. As per the BET measurements, there was an increase in the surface area from 13.507 m^2/g (IRMOF-9) to 38.410 m^2/g ($Pd_{10\%}$@IRMOF-9). Moreover, there was ∼2-fold enhancement in the average pore diameter of $Pd_{10\%}$@IRMOF-9 (13.59 to 24.23 nm). The increase in the surface area and pore volume may account for the increased catalytic efficiency of the $Pd_{10\%}$@IRMOF-9 material toward the reductive degradation of dyes.

The surface morphology of IRMOF-9 and Pd_x@IRMOF-9 (*x* = 2, 5, and 10%) was analyzed by SEM. In the case of IRMOF-9, micrometer-sized sheet-like structures of about 3−4 μm in length and 1−1.5 μm in width were obtained, as can be observed from Figure 2a. These sheet-like structures resulted in flower-like morphologies upon incorporation of Pd(II) in IRMOF-9. In the case of $Pd_{2\%}$@IRMOF-9, the sheets of IRMOF-9 appeared as flower-like structures of ∼2 μm in size having petals spaced wide apart, as shown in Figure 2b, while in the case of $Pd_{5\%}$@IRMOF-9, ∼5−6 μm size flowers were obtained (Figure 2c). With increasing concentration of Pd(II) loading (2−5%), the size of the flower increased along with the increase in the petal density. In the case of $Pd_{10\%}$@IRMOF-9, spherical cauliflower-like MOFs (∼8−9 μm) were obtained (Figure 2d). These cauliflower-shaped MOFs are nanoporous in nature (∼500−600 nm), as can be noticed from Figure 2e,f. The EDX analysis of $Pd_{10\%}$@IRMOF-9 showed the presence of Pd along with other components such as Zn, C, and O (Figure 2i). The area mapping of the $Pd_{10\%}$@IRMOF-9 material suggested that Pd(II) is homogeneously distributed over the MOF material (Figure 2g,h). The merged mapped image of $Pd_{10\%}$@IRMOF-9 is given in Figure 2h, and the individual area mapping for each element is given in the Supporting Information SI.01, Figure S01. The area mapping and EDX analysis for IRMOF-9 showed the presence of Zn, C, and O, as shown in Figure S02 in SI.02. Based on the surface morphology of all the synthesized Pd-loaded MOFs, $Pd_{10\%}$@IRMOF-9 was selected for investigation of the catalytic activity toward dye degradation.

$Pd_{10\%}$@IRMOF-9-Catalyzed Reductive Degradation of Organic Dyes. The degradation studies were performed on cationic dyes, namely, methylene blue (MB) and rhodamine 6G (R6G); anionic dyes, such as congo red (CR) and orange G (OG); and neutral dyes such as neutral red, by using $NaBH_4$

https://doi.org/10.1021/acsomega.3c03014
ACS Omega 2023, 8, 38895−38904

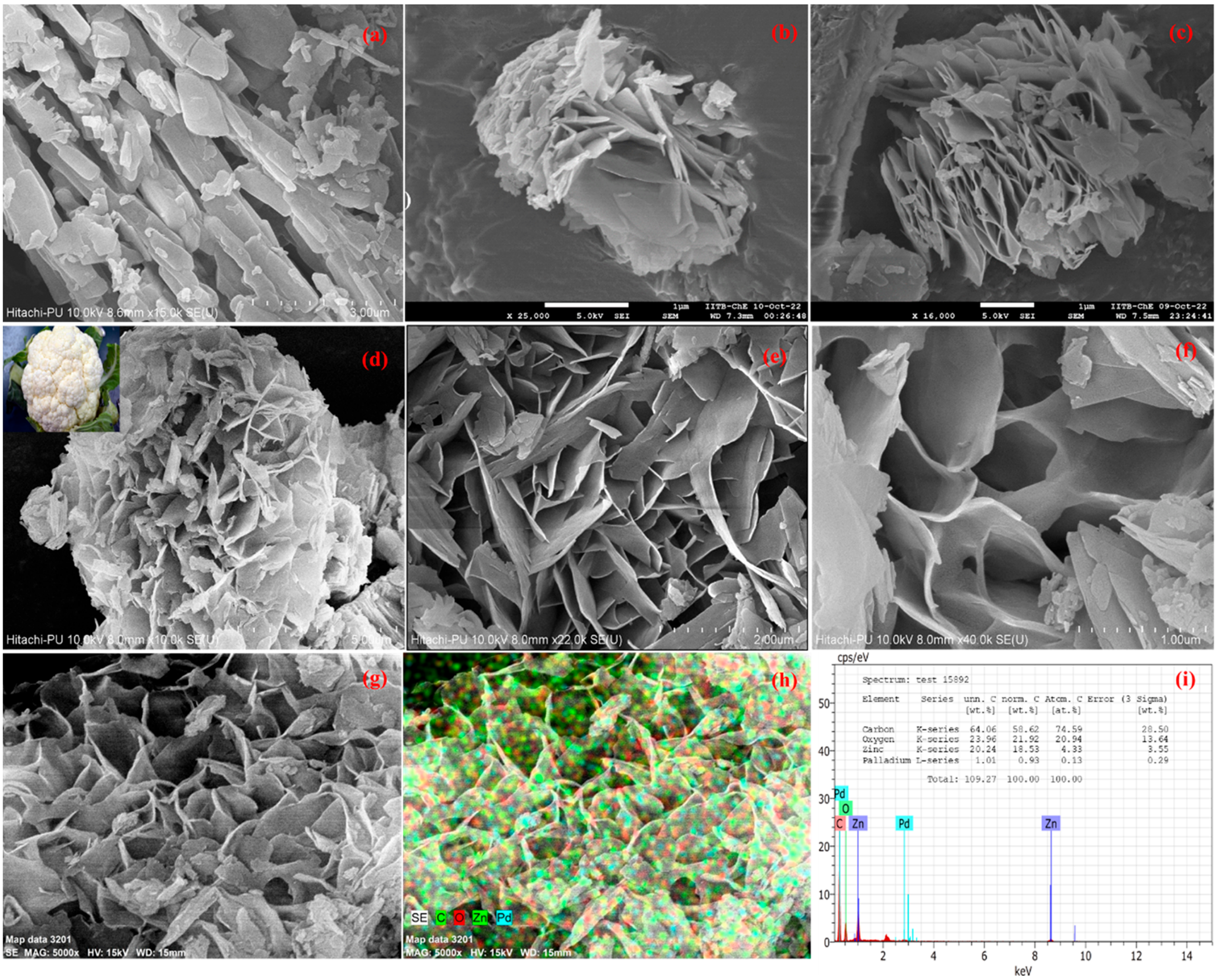

Figure 2. SEM images of (a) IRMOF-9, (b) $Pd_{2\%}$@IRMOF-9, (c) $Pd_{5\%}$@IRMOF-9, and (d) $Pd_{10\%}$@IRMOF-9 (the inset image shows the comparison with the cauliflower-like structure); (e,f) enlarged images of $Pd_{10\%}$@IRMOF-9 showing the petal density and the porosity; (g) image of $Pd_{10\%}$@IRMOF-9 selected for area mapping; (h) SEM-mapped monograph; (i) EDX analysis showing the presence of all the elements in the case of $Pd_{10\%}$@IRMOF-9. The scale bar in the case of (a−f) is 3, 1, 1, 5, 2, and 1 μm, respectively.

as a reducing agent. The absorption spectra of CR, MB, MO, NR, R6G, OG, and MR showed λ_{max} values at 497, 664, 464, 451, 526, 480, and 425 nm, respectively. The time taken by the material, $Pd_{10\%}$@IRMOF-9, for the degradation of the dyes varied irrespective of the charge on the dyes. The reductive degradation time taken for CR, MO, MR, OG, NR, MB, and R6G was found to be 15, 31, 20, 23, 8 min, 40 s, and 45 min, respectively (Figure 3a−g). Plots of absorbance *vs* time for all the dyes are given in the Supporting Information SI.03, Figure S03. Further, the degradation efficiency of the MOF material was calculated by using the following expression:

Degradation efficiency = $(1 - C_t/C_0) \times 100$, where "C_0" is the initial concentration and "C_t" is the concentration of the dyes after a certain time.

The degradation efficiency and time taken for degradation by the MOF material, i.e., $Pd_{10\%}$@IRMOF-9 for various dyes are given in Figure 3h, i. The degradation efficiency was found to be higher than 95% for OG, MB, and MO. While for CR, MR, R6G, and NR, the degradation efficiency was found to be >90%, as can be noticed from Figure 3h. These results confirm that the synthesized $Pd_{10\%}$@IRMOF-9 is a robust and efficient material for the degradation of dyes of diverse nature.

Kinetic Study of the Degradation of Dyes. The absorption studies support that the degradation of dyes followed pseudo-first-order kinetics. The kinetic calculations of all of the dyes were carried out by using a first-order rate equation:

$\ln(C_t/C_0) = -Kt + c$, where 't' is the reaction time, 'K' is the rate constant, "C_0" is the initial concentration, and "C_t" is the concentration at time t. The value for the rate constant, K, was obtained from the slope of the linear plot of the graph between $\ln(C_t/C_0)$ vs t.

Effect of $Pd_{10\%}$@IRMOF-9 Concentration. To calculate the kinetic parameters, the effect of various concentrations of $Pd_{10\%}$@IRMOF-9 on the degradation of CR dye was studied in the concentration range from 1.04 to 10.578 μg/mL. The values of rate constant obtained by varying the $Pd_{10\%}$@IRMOF-9 concentration from 1.04 to 2.631, 4.22, 5.89, 7.39, and 10.57 μg/mL were found to be 0.35×10^{-1}, 1.069×10^{-1}, 1.39×10^{-1}, 3.69×10^{-1}, 6.04×10^{-1}, and 3.59×10^{-1} min^{-1} respectively, Figure 4a−f. A significant increase in the rate of

https://doi.org/10.1021/acsomega.3c03014
ACS Omega 2023, 8, 38895−38904

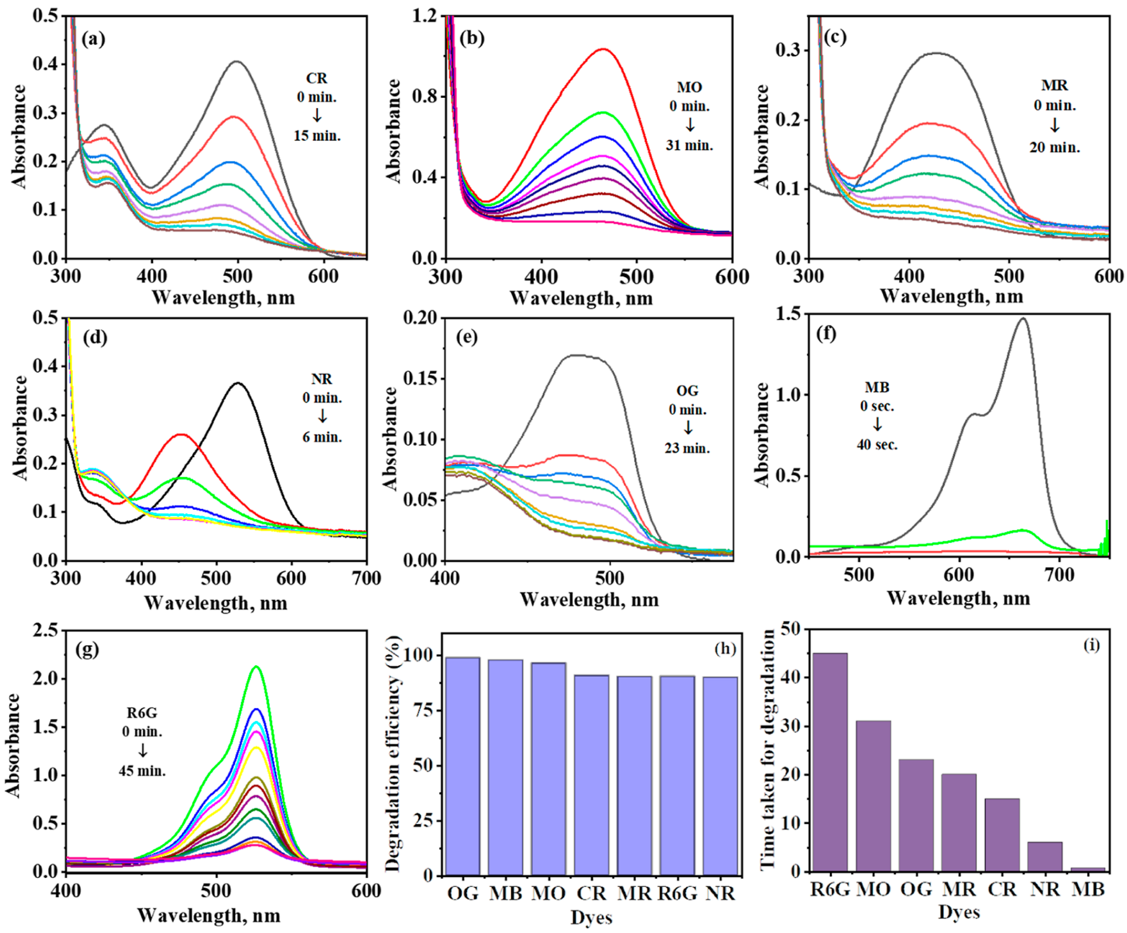

Figure 3. Absorption spectra of various organic dyes using $Pd_{10\%}$@IRMOF-9 material in the presence of $NaBH_4$: (a) CR, (b) MO, (c) MR, (d) NR, (e) OG, (f) MB, and (g) R6G; (h), (i) % degradation efficiency and the time taken for all the dyes studied, respectively. Reaction conditions: dye concentration, 22.5 μM; $NaBH_4$, 0.83 mM; $Pd_{10\%}$@IRMOF-9 concentration, 0.083 mg/mL.

degradation of CR dye was observed with an increase in the concentration of $Pd_{10\%}$@IRMOF-9 up to 7.3 μg/mL. Further, the increase in the material concentration resulted in a small decrease in the rate of reaction, as can be noticed from Figure 4g. Steady-state kinetic parameters were evaluated by changing the concentration of the material, viz., $Pd_{10\%}$@IRMOF-9. From the absorption vs time plot, the initial velocity was calculated by using the equation, $V_{initial} = slope_{initial}/\varepsilon$. The plot of velocity as a function of catalyst concentration showed a typical Michaelis−Menten saturation curve, plotted in Figure 4h. The reaction rate increased gradually with increasing $Pd_{10\%}$@IRMOF-9 concentration until it reaches the maximum value, 6.04×10^{-1} min^{-1}, indicating the saturation in the reactivity of $Pd_{10\%}$@IRMOF-9. Michelis−Menten parameters K_m and V_{max} were calculated from the double reciprocal Lineweaver−Burk plot, and their values were found to be 13.26 μM and 26.68×10^{-8} M min^{-1}, respectively. The absorption spectra and absorbance vs time plots recorded by varying the concentration of the catalyst are given in Supporting Information SI.04, Figure S04, and SI.05, Figure S05, respectively.

Control experiments for the degradation of dyes were performed with $NaBH_4$ (0.01 M) and IRMOF-9. The absorption spectra of CR dye were measured and monitored for 45 min in the presence of $NaBH_4$ alone as well as with $NaBH_4$/IRMOF-9. The spectral data for these are given in the Supporting Information SI.06, Figure S06. The bar diagram given in Figure 5a depicts the comparison of the % degradation of CR dye in the case of $NaBH_4$, $NaBH_4$/IRMOF-9, and $Pd_{10\%}$@IRMOF-9. IRMOF-9 and $NaBH_4$/IRMOF-9 degraded the CR dye up to 2% which is about 1/44th of the catalytic efficiency of $Pd_{10\%}$@IRMOF-9. The rate constant for all the other dyes was also calculated by using the equation $\ln(C_t/C_0) = -Kt + c$, and these parameters are defined above in the kinetic calculations. The values of the rate constant for MB, MO, MR, OG, R6G, NR, and CR were found to be 54.1×10^{-1}, 5.42×10^{-2}, 6.37×10^{-2}, 8.14×10^{-2}, 4.63×10^{-2}, 3.47×10^{-1}, and 1×10^{-1} min^{-1}, respectively (Figure 5b). The plot of $\ln(C_t/C_0)$ vs time for all of the dyes are given in the Supporting Information SI.07, Figure S07. The rate of degradation of the dyes by using $Pd_{10\%}$@IRMOF-9 was found to be independent of the nature of and charge on the dyes. The rate constant of the neutral dye is ∼1.5−2 times higher than those of anionic dyes, MO, MR, OG, and CR. However, the rate constant of MB dye (cationic) is ∼16 times higher than the NR. The value of $t_{1/2}$ was calculated by the equation $t_{1/2} = 0.693/K$, where K is the rate constant of the respective dyes. The values of $t_{1/2}$ for R6G, MO, MR, OG, CR, NR, and MB were found to be 0.1497, 0.128, 0.108, 0.0851, 0.0693, 0.01997, and 0.001348 min, respectively, as can be noticed from Figure 5c. The bar graph depicts that the value of $t_{1/2}$ follows the order: anionic > neutral > cationic dyes.

The recyclability of the MOF material, i.e., $Pd_{10\%}$@IRMOF-9 was further explored for a few consecutive cycles. The degradation of CR dye was checked by using the recovered

https://doi.org/10.1021/acsomega.3c03014
ACS Omega 2023, 8, 38895−38904

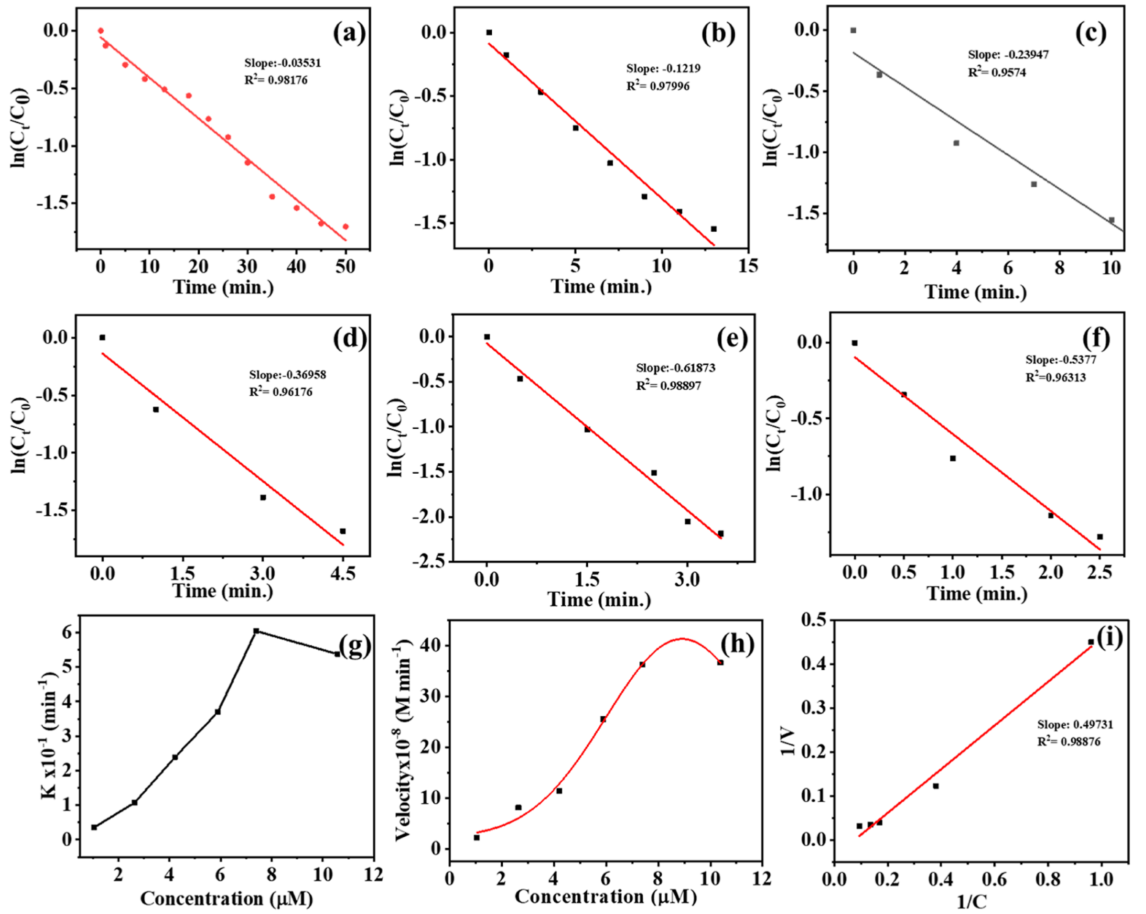

Figure 4. Plot of ln C_t/C_0 vs time for (a) 1.04, (b) 2.631, (c) 4.2, (d) 5.89, (e) 7.39, and (f) 10.578 μg/mL; (g) rate constant vs varying concentration of $Pd_{10\%}$@IRMOF-9; (h) steady-state kinetics; (i) double reciprocal plot for the calculation of enzyme kinetic parameters by varying the concentration of $Pd_{10\%}$@IRMOF-9. Reaction conditions: dye concentration, 22.5 μM; $NaBH_4$, 0.83 mM; Pd(II) in $Pd_{10\%}$@IRMOF-9 concentration, 1.04−10.578 μg/mL.

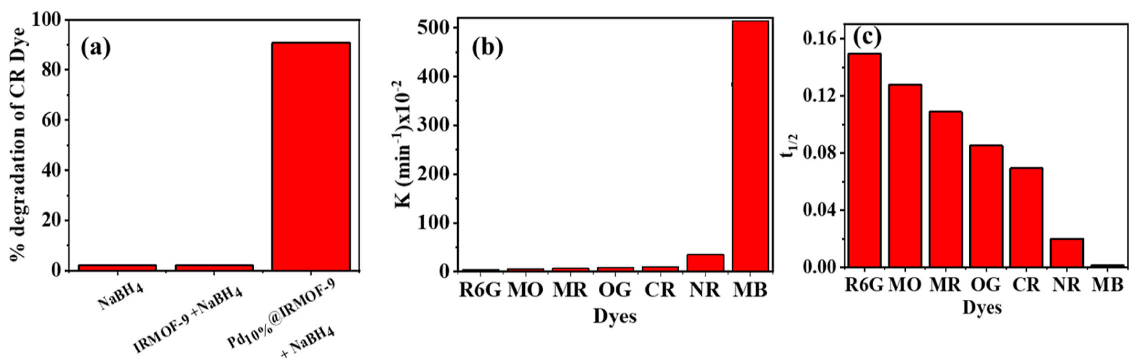

Figure 5. Bar diagram of (a) % degradation of CR dye in the presence of $NaBH_4$, $NaBH_4$ + IRMOF-9, and $NaBH_4$ + $Pd_{10\%}$IRMOF-9; (b) rate constant K of various dyes; (c) $t_{1/2}$ of all the dyes studied.

material from the previous set of reactions. $Pd_{10\%}$@IRMOF-9 showed recyclability up to five consecutive cycles without significant loss in the catalytic activity. A minor decrease in the efficiency of the material, i.e., $Pd_{10\%}$@IRMOF-9 was observed after the third cycle, as shown in Figure 6a. The bar diagram illustrates that the recycled catalytic material degraded CR dye >87% for first three cycles. However, the % degradation of CR dye decreased to ∼70% in the last cycle. The recycled material was characterized by PXRD to confirm any structural changes. PXRD of the recycled material indicates additional peaks at 2θ = 40 and 45° that correspond to the (111) and (200) planes due to conversion of Pd (II) into Pd(0) (Figure 6b). To confirm the presence of Pd (0) in $Pd_{10\%}$@IRMOF-9, XPS analysis was performed. The XPS spectrum of $Pd_{10\%}$@IRMOF-9 showed the presence of Pd (II) and Pd(0) peaks of $3d_{5/2}$ and $3d_{3/2}$ at 332.98, 339.49 eV and 334.64, 338.01 eV, respectively (Figure 6c). The agglomeration of Pd(0) species on the surface of IRMOF-9 due to recycling may account for the decrease in the efficiency of the material.

Further, a plausible mechanism of the degradation of dyes using Pd(II)@IRMOF-9 is outlined in Scheme 2.

https://doi.org/10.1021/acsomega.3c03014
ACS Omega 2023, 8, 38895−38904

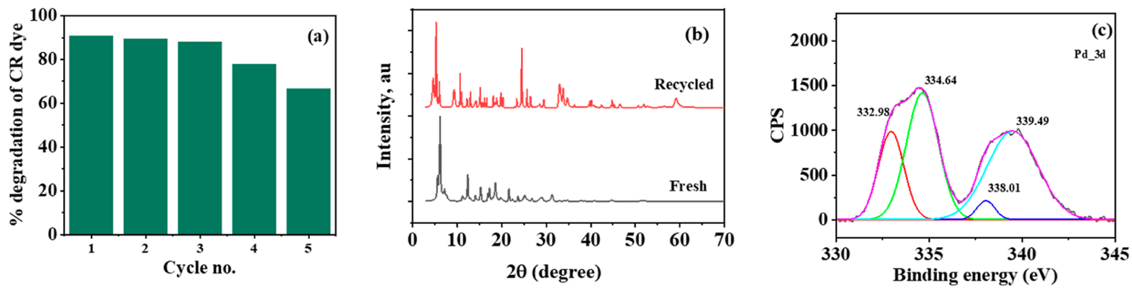

Figure 6. (a) Bar graph depicting the recyclability studies of $Pd_{10\%}$@IRMOF-9 for the degradation of CR dye; (b) comparison of PXRD of the fresh and the recycled material; (c) XPS spectra of the recycled material, $Pd_{10\%}$@IRMOF-9.

Scheme 2. Plausible Mechanism for Dye Degradation

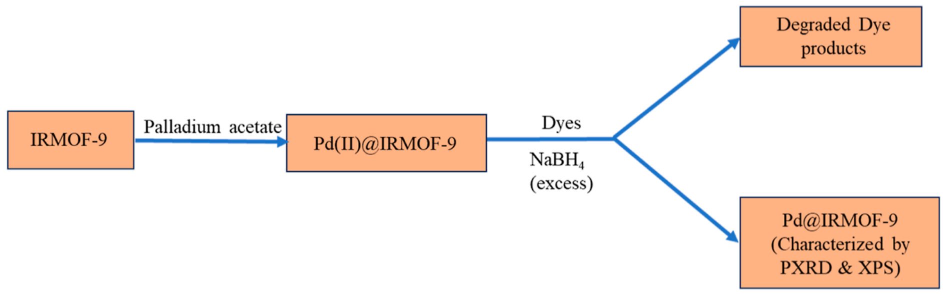

Table 1. Comparison of Degradation Efficiency of $Pd_{10\%}$@IRMOF-9 with Those of Existing Catalysts

catalyst	catalyst concentration	dye studied	degradation time	reference
heteroatom@ZIF-67	20 mg	CR and MO	30−60 min	49
CA-AgNPs	1 mg	CR and MB	36 min and 32 min	50
CuO@C	12 mg	CR and MB	55 min and 15 min	51
Fe_3O_4@silica Pd NPs	0.4 mg	MO, MR, and MB	20 min	52
MR assisted Pd NPs	4 mg	CR	14 min	53
MTiCuPd500	5 mg	MB	20 min	54
Pd/CNF	10 mg	MO	240 min	55
$NiFe_2O_4/\gamma$-Fe_2O_3	0.1 mg	MO	36 min	56
$CoFe_2O_4/\gamma$-Fe_2O_3	0.1 mg	MO	36 min	56
Pd/ZSM-5 & Pd/MMZ	0.5 mg	MB	12 and 3 min	57
MnO_2. RGO	10 mg	NR	90 min	58
Zn/CeO_2	10 μM	NR	60 min	59
Fe/Pd NPs	0.1−2.0 g/L	orange II	12 min	60
$Pd_{10\%}$@IRMOF-9	2.631 μg	CR, MR, MO, NR, MB, OG, and R6G	15 min, 20 min, 31 min, 6 min, 40 s, 23 min, and 45 min	present work

A comparative statement of the catalytic efficiency of the synthesized material with respect to the existing catalysts, in terms of catalytic concentration and degradation time, is presented in Table 1 which signifies the robustness of the material $Pd_{10\%}$@IRMOF-9.

■ CONCLUSIONS

Organic dyes have been extensively used across the globe, and release of these dyes into water bodies causes serious health problems. Various types of MOFs have been reported for the removal and degradation of organic dyes from water. However, the zinc-based MOF, IRMOF-9, has not been explored toward dye degradation until now. In this regard, a series of Pd-doped IRMOF-9, $Pd_{2\%}$@IRMOF-9, $Pd_{5\%}$@IRMOF-9, and $Pd_{10\%}$@IRMOF-9, were synthesized by varying the concentration of palladium acetate on IRMOF-9 using the impregnation technique. These MOFs were characterized by various characterization techniques such as FT-IR, UV−Vis, PXRD, and SEM analyses. The PXRD data of all three $Pd_{x\%}$@IRMOF-9 are in line with IRMOF-9, which suggests no structural change even after the loading of Pd(II) and that is further supported by FTIR and UV−vis spectra. The BET measurements showed enhancements in the surface area and pore diameter of $Pd_{10\%}$@IRMOF-9. The surface morphology of IRMOF-9 and $Pd_{10\%}$@IRMOF-9, analyzed using SEM, illustrated the initial formation of a flower-like structure which develops as a cauliflower-shaped porous MOF of ∼8 μm size. Based on the surface morphology of Pd(II)-loaded MOFs, $Pd_{10\%}$@IRMOF-9 was employed for the degradation of seven organic dyes due to the high petal density and porous framework. A brief summary of the synthesis, characterization, and reductive degradation of organic dyes using $Pd_{10\%}$IRMOF-9 material is depicted in Scheme 3.

Kinetic studies of all these dyes were calculated by using the equation $\ln(C_t/C_0) = -Kt + c$, which follows pseudo first-order kinetics. The $t_{1/2}$ of all these dyes, viz., CR, MO, MR, R6G, MB, OG, and NR was found to be 0.0693, 0.127, 0.1088,

https://doi.org/10.1021/acsomega.3c03014
ACS Omega 2023, 8, 38895−38904

Scheme 3. Brief Outlook of the Synthesis, Characterization, and Reductive Degradation of Organic Dyes Using $Pd_{10\%}$IRMOF-9 Material

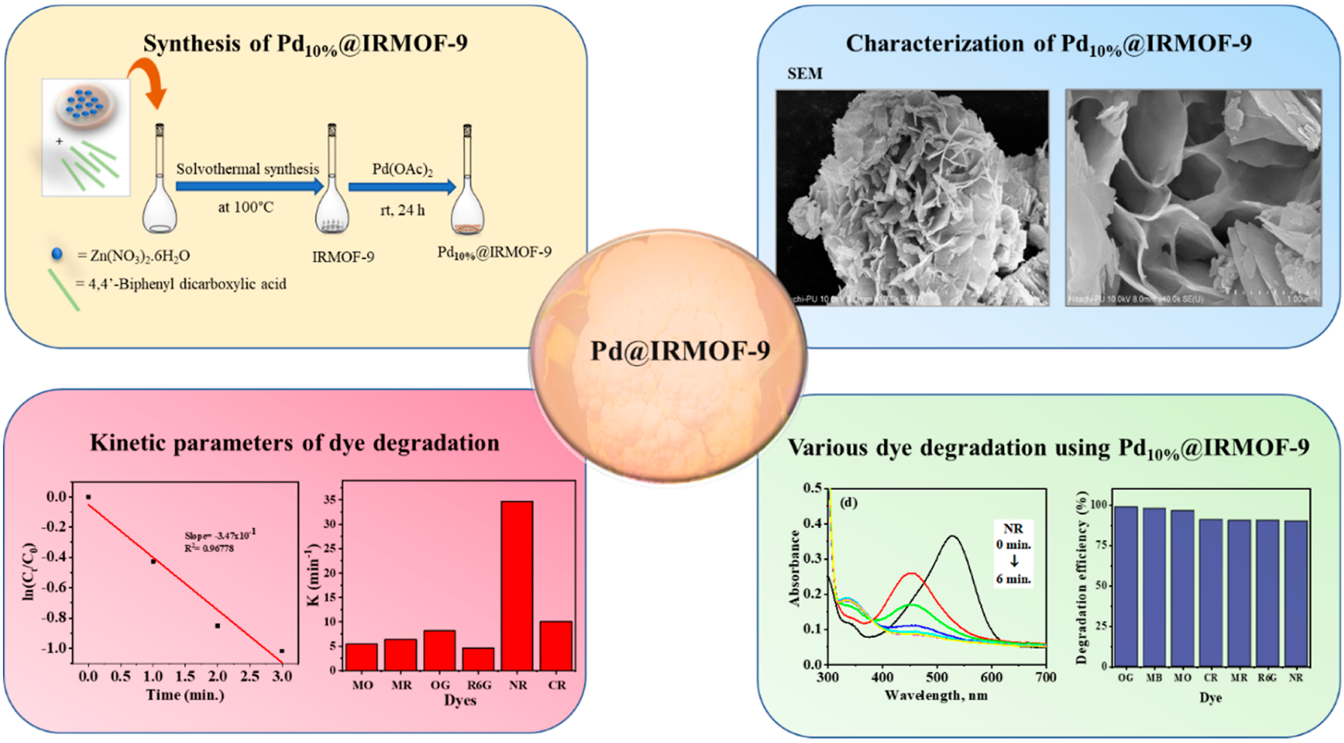

0.14967, 0.00134, 0.085, and 0.01997 min, respectively. K_M and V_{max} values were calculated by the steady-state approximation and found to be 13.2 μM and 26.68 $\times$ 10^{-8} M min^{-1}, respectively.

In summary, we have developed a robust and efficient material that can be effectively utilized for the degradation of organic dyes in an aqueous medium which can be recycled for up to five consecutive cycles.

■ ASSOCIATED CONTENT

Supporting Information

The Supporting Information is available free of charge at https://pubs.acs.org/doi/10.1021/acsomega.3c03014.

Absorption spectral data of degradation of various dyes and the area mapping and elemental analysis of the material (PDF)

■ AUTHOR INFORMATION

Corresponding Authors

Bhawna Uttam – *Department of Chemistry, J.C. Bose University of Science and Technology, YMCA, Faridabad 121006, India*; orcid.org/0000-0002-7031-318X; Email: bhawnauttamchem@gmail.com

Ravi Kumar – *Department of Chemistry, J.C. Bose University of Science and Technology, YMCA, Faridabad 121006, India*; Email: ravi.dhamija@rediffmail.com

Authors

Rimi – *Department of Chemistry, J.C. Bose University of Science and Technology, YMCA, Faridabad 121006, India*

Pardeep Kumar – *Department of Chemical Engineering, University of Virginia, Charlottesville, Virginia 22904, United States*

Complete contact information is available at: https://pubs.acs.org/10.1021/acsomega.3c03014

Notes

The authors declare no competing financial interest.

■ ACKNOWLEDGMENTS

B.U. and R.K. acknowledge financial support from DST, Haryana {HSCSIT/R&D/2022/164}. R.K. is grateful to J. C. Bose University of Science & Technology for the seed grant {R&D/SG/2020-21/166}and DST, Government of India for the DST-PURSE grant {SR/PURSE/2022/126}. B.U. is also thankful to DST, Government of India for the SERB-POWER Grant, {SPG/2021/004027}. Rimi acknowledges J. C. Bose University of Science & Technology for the award of University Research Fellowship. We acknowledge the Central Instrumentation Laboratories (CIL) of J. C. Bose University of Science & Technology for providing the instrumentation facilities.

■ REFERENCES

(1) Butova, V. V. E.; Soldatov, M. A.; Guda, A. A.; Lomachenko, K. A.; Lamberti, C. Metal-organic frameworks: structure, properties, methods of synthesis and characterization. *Russ. Chem. Rev.* **2016**, *85*, 280–307.

(2) Yuan, S.; Feng, L.; Wang, K.; Pang, J.; Bosch, M.; Lollar, C.; Sun, Y.; Qin, J.; Yang, X.; Zhang, P.; Wang, Q.; Zou, L.; Zhang, Y.; Zhang, L.; Fang, Y.; Li, J.; Zhou, H. C. Stable metal-organic frameworks: design, synthesis, and applications. *Adv. Mater.* **2018**, *30*, 1704303.

(3) Dohi, T.; Zhdankin, V. V.; Kumar, R.; Rimi, R.; Soni, S.; Uttam, B.; China, H. Recyclable hypervalent iodine reagents in modern organic synthesis. *Synthesis* **2022**, *54*, 2731–2748.

(4) Liu, J.; Chen, L.; Cui, H.; Zhang, J.; Zhang, L.; Su, C. Y. Applications of metal-organic frameworks in heterogeneous supramolecular catalysis. *Chem. Soc. Rev.* **2014**, *43*, 6011–6061.

(5) Guo, J.; Qin, Y.; Zhu, Y.; Zhang, X.; Long, C.; Zhao, M.; Tang, Z. Metal-organic frameworks as catalytic selectivity regulators for organic transformations. *Chem. Soc. Rev.* **2021**, *50*, 5366−5396.

(6) Jiao, L.; Wang, Y.; Jiang, H. L.; Xu, Q. Metal-organic frameworks as platforms for catalytic applications. *Adv. Mater.* **2018**, *30*, 1703663.

(7) Hao, M.; Qiu, M.; Yang, H.; Hu, B.; Wang, X. Recent advances on preparation and environmental applications of MOF-derived carbons in catalysis. *Sci. Total Environ.* **2021**, *760*, 143333.

(8) Horcajada, P.; Gref, R.; Baati, T.; Allan, P. K.; Maurin, G.; Couvreur, P.; Férey, G.; Morris, R. E.; Serre, C. Metal-organic frameworks in biomedicine. *Chem. Rev.* **2012**, *112*, 1232−1268.

(9) Chen, X.; Li, M.; Lin, M.; Lu, C.; Kumar, A.; Pan, Y.; Liu, J.; Peng, Y. Current and promising applications of Hf (IV)-based MOFs in clinical cancer therapy. *J. Mater. Chem. B* **2023**, *11*, 5693−5714.

(10) Mendes, R. F.; Figueira, F.; Leite, J. P.; Gales, L.; Almeida Paz, F. A. Metal-organic frameworks: a future toolbox for biomedicine? *Chem. Soc. Rev.* **2020**, *49*, 9121−9153.

(11) Chen, J.; Zhang, Z.; Ma, J.; Nezamzadeh-Ejhieh, A.; Lu, C.; Pan, Y.; Liu, J.; Bai, Z. Current status and prospects of MOFs in controlled delivery of Pt anticancer drugs. *Dalton Trans.* **2023**, *52*, 6226−6238.

(12) Li, Y.; Li, D.; Qin, T.; Shi, Z.; Fu, P.; Xiong, D.; Dong, X. A comparative study of proton conduction between two new Cd (II) and Co (II) complexes and in vitro antibacterial study of the Cd (II) complex. *Appl. Organomet. Chem.* **2023**, *37*, No. e6920.

(13) Liu, X.; Yang, H.; Diao, Y.; He, Q.; Lu, C.; Singh, A.; Kumar, A.; Liu, J.; Lan, Q. Recent advances in the electrochemical applications of Ni-based metal-organic frameworks (Ni-MOFs) and their derivatives. *Chemosphere* **2022**, *307*, 135729.

(14) Wang, B.; Xie, L. H.; Wang, X.; Liu, X. M.; Li, J.; Li, J. R. Applications of metal-organic frameworks for green energy and environment: New advances in adsorptive gas separation, storage and removal. *Green Energy Environ.* **2018**, *3*, 191−228.

(15) Jia, T.; Gu, Y.; Li, F. Progress and potential of metal-organic frameworks (MOFs) for gas storage and separation: A review. *J. Environ. Chem. Eng.* **2022**, *10*, 108300.

(16) Fan, W.; Zhang, X.; Kang, Z.; Liu, X.; Sun, D. Isoreticular chemistry within metal-organic frameworks for gas storage and separation. *Coord. Chem. Rev.* **2021**, *443*, 213968.

(17) Uddin, M. J.; Ampiaw, R. E.; Lee, W. Adsorptive removal of dyes from wastewater using a metal-organic framework: A review. *Chemosphere* **2021**, *284*, 131314.

(18) Drout, R. J.; Robison, L.; Chen, Z.; Islamoglu, T.; Farha, O. K. Zirconium metal-organic frameworks for organic pollutant adsorption. *Trends Chem.* **2019**, *1*, 304−317.

(19) Ke, F.; Pan, A.; Liu, J.; Liu, X.; Yuan, T.; Zhang, C.; Fu, G.; Peng, C.; Zhu, J.; Wan, X. Hierarchical camellia-like metal-organic frameworks via a bimetal competitive coordination combined with alkaline-assisted strategy for boosting selective fluoride removal from brick tea. *J. Colloid Interface Sci.* **2023**, *642*, 61−68.

(20) Ibrahim, A. O.; Adegoke, K. A.; Adegoke, R. O.; Abdul Wahab, Y. A.; Oyelami, V. B.; Adesina, M. O. Adsorptive removal of different pollutants using metal-organic framework adsorbents. *J. Mol. Liq.* **2021**, *333*, 115593.

(21) Dong, X.; Li, Y.; Li, D.; Liao, D.; Qin, T.; Prakash, O.; Kumar, A.; Liu, J. A new 3D 8-connected Cd(II) MOF as a potent photocatalyst for oxytetracycline antibiotic degradation. *CrystEngComm* **2022**, *24*, 6933−6943.

(22) Jin, J. C.; Wang, J.; Guo, J.; Yan, M. H.; Wang, J.; Srivastava, D.; Kumar, A.; Sakiyama, H.; Muddassir, M.; Pan, Y. A 3D rare cubane-like tetramer Cu (II)-based MOF with 4-fold dia topology as an efficient photocatalyst for dye degradation. *Colloids Surf., A* **2023**, *656*, 130475.

(23) Kang, W.; Zhong, W.; Li, C.; Xia, F.; Wu, Y.; Prakash, O.; Kumar, A.; Sakiyama, H.; Muddassir, M. Photocatalytic properties of two new isostructural cobalt(II) and nickel(II) complexes having terphenyl-3,3″,4,4″-teteacarboxylic acid. *Polyhedron* **2022**, *228*, 116158.

(24) Xiong, M.; Wu, J.; Lu, L.; Wang, J.; Zhang, W.; Guo, J.; Singh, A.; Kumar, A.; Muddassir, M. Construction strategies to modulate the photocatalytic efficiency of Cd (ii) MOFs to photodegrade organic dyes. *CrystEngComm* **2022**, *24* (45), 7986−7995.

(25) Juan-Alcaniz, J.; Gascon, J.; Kapteijn, F. Metal-organic frameworks as scaffolds for the encapsulation of active species: state of the art and future perspectives. *J. Mater. Chem.* **2012**, *22*, 10102−10118.

(26) Yadav, M.; Aijaz, A.; Xu, Q. Highly catalytically active palladium nanoparticles incorporated inside metal-organic framework pores by double solvents method. *Funct. Mater. Lett.* **2012**, *05*, 1250039.

(27) Yang, Q.; Yao, F.; Zhong, Y.; Chen, F.; Shu, X.; Sun, J.; He, L.; Wu, B.; Hou, K.; Wang, D.; Li, X. Metal-Organic Framework Supported Palladium Nanoparticles: Applications and Mechanisms. *Part. Part. Syst. Char.* **2019**, *36*, 1800557.

(28) Abdel-Mageed, A. M.; Rungtaweevoranit, B.; Parlinska-Wojtan, M.; Pei, X.; Yaghi, O. M.; Behm, R. J. Highly active and stable single-atom Cu catalysts supported by a metal-organic framework. *J. Am. Chem. Soc.* **2019**, *141*, 5201−5210.

(29) Esrafili, L.; Morsali, A.; Dehghani Firuzabadi, F.; Retailleau, P. Development of porous cobalt-/copper-doped carbon nanohybrids derived from functionalized MOFs as efficient catalysts for the Ullmann cross-coupling reaction: Insights into the active centers. *ACS Appl. Mater. Interfaces* **2020**, *12*, 43115−43124.

(30) Aijaz, A.; Xu, Q. Catalysis with metal nanoparticles immobilized within the pores of metal-organic frameworks. *J. Phys. Chem. Lett.* **2014**, *5*, 1400−1411.

(31) Malik, A.; Nath, M. Ultrafast catalytic reduction of toxic nitroaromatics and organic colouring dyes by using Au/ZIF-11: Efficient wastewater treatment. *J. Water Process Eng.* **2021**, *44*, 102362.

(32) Haleem, A.; Shafiq, A.; Chen, S. Q.; Nazar, M. A. A Comprehensive Review on Adsorption, Photocatalytic and Chemical Degradation of Dyes and Nitro-Compounds over Different Kinds of Porous and Composite Materials. *Molecules* **2023**, *28*, 1081.

(33) Ndolomingo, M. J.; Bingwa, N.; Meijboom, R. Review of supported metal nanoparticles: synthesis methodologies, advantages and application as catalysts. *J. Mater. Sci.* **2020**, *55*, 6195−6241.

(34) Haseena, M.; Malik, M. F.; Javed, A.; Arshad, S.; Asif, N.; Zulfiqar, S.; Hanif, J. Water pollution and human health. *Environ. Risk Assess. Rem.* **2017**, *1*, 16−19.

(35) Al-Tohamy, R.; Ali, S. S.; Li, F.; Okasha, K. M.; Mahmoud, Y. A. G.; Elsamahy, T.; Jiao, H.; Fu, Y.; Sun, J. A critical review on the treatment of dye-containing wastewater: Ecotoxicological and health concerns of textile dyes and possible remediation approaches for environmental safety. *Ecotoxicol. Environ. Saf.* **2022**, *231*, 113160.

(36) Affat, S. S. Classifications, advantages, disadvantages, toxicity effects of natural and synthetic dyes: a review. *Univ. Thi-Qar J.* **2021**, *8*, 130−135.

(37) Xiao, W.; Jiang, X.; Liu, X.; Zhou, W.; Garba, Z. N.; Lawan, I.; Wang, L.; Yuan, Z. Adsorption of organic dyes from wastewater by metal-doped porous carbon materials. *J. Clean. Prod.* **2021**, *284*, 124773.

(38) Dong, X.; Shi, Z.; Li, D.; Li, Y.; An, N.; Shang, Y.; Sakiyama, H.; Muddassir, M.; Si, C. The regulation research of topology and magnetic exchange models of CPs through Co (II) concentration adjustment. *J. Solid State Chem.* **2023**, *318*, 123713.

(39) Narkhede, N.; Uttam, B.; Rao, C. P. Calixarene-Assisted Pd Nanoparticles in Organic Transformations: Synthesis, Characterization, and Catalytic Applications in Water for C-C Coupling and for the Reduction of Nitroaromatics and Organic Dyes. *ACS Omega* **2019**, *4*, 4908−4917.

(40) Polepalli, S.; Uttam, B.; Rao, C. P. Protein-inorganic nano hybrid sheets of Pd embedded BSA as a robust catalyst in water for oxidase mimic activity and C-C coupling reactions, and as a sustainable material for micromolar sensing of dopamine. *Adv. Mater.* **2020**, *1*, 2074−2083.

(41) Du, Q.; Rao, R.; Bi, F.; Zhang, X.; Liu, N.; Yang, Y.; Zhang, W.; Yang, Y.; Liu, N.; Zhang, X. Preparation of modified zirconium-based metal-organic frameworks (Zr-MOFs) supported metals and recent application in environment: a review and perspectives. *Surface. Interfac.* **2022**, *28*, 101647.

(42) Roy, D.; Kumar, P.; Soni, A.; Nemiwal, M. A versatile and microporous Zn-based MOFs as a recyclable and sustainable heterogeneous catalyst for various organic transformations: A review (2015-present). *Tetrahedron* **2023**, *138*, 133408.

(43) Eddaoudi, M.; Kim, J.; Rosi, N.; Vodak, D.; Wachter, J.; O'Keeffe, M.; Yaghi, O. M. Systematic design of pore size and functionality in isoreticular MOFs and their application in methane storage. *Science* **2002**, *295*, 469−472.

(44) Lin, C. K.; Zhao, D.; Gao, W. Y.; Yang, Z.; Ye, J.; Xu, T.; Ge, Q.; Ma, S.; Liu, D. J. Tunability of band gaps in metal-organic frameworks. *Inorg. Chem.* **2012**, *51*, 9039−9044.

(45) Bryant, M. R.; Burrows, A. D.; Kepert, C. J.; Southon, P. D.; Qazvini, O. T.; Telfer, S. G.; Richardson, C. Mixed-Component Sulfone-Sulfoxide Tagged Zinc IRMOFs: In Situ Ligand Oxidation, Carbon Dioxide, and Water Sorption Studies. *Cryst. Growth Des.* **2017**, *17*, 2016−2023.

(46) Babarao, R.; Coghlan, C. J.; Rankine, D.; Bloch, W. M.; Gransbury, G. K.; Sato, H.; Kitagawa, S.; Sumby, C. J.; Hill, M. R.; Doonan, C. J. Does functionalisation enhance CO_2 uptake in interpenetrated MOFs? An examination of the IRMOF-9 series. *Chem. Commun.* **2014**, *50*, 3238−3241.

(47) Dau, P. V.; Cohen, S. M. A bifunctional, site-isolated metal-organic framework-based tandem catalyst. *Inorg. Chem.* **2015**, *54*, 3134−3138.

(48) Bryant, M. R.; Richardson, C. Hypervalent organoiodine (v) metal-organic frameworks: syntheses, thermal studies, and stoichiometric oxidants. *Dalton Trans.* **2020**, *49*, 5167−5174.

(49) Abdellatif, A. B. A.; El-Bery, H. M.; Abdelhamid, H. N.; El-Gyar, S. A. ZIF-67 and Cobalt-based@ heteroatom-doped carbon nanomaterials for hydrogen production and dyes removal via adsorption and catalytic degradation. *J. Environ. Chem. Eng.* **2022**, *10*, 108848.

(50) Alamier, W. M.; Hasan, N.; Ali, S. K.; Oteef, M. D. Biosynthesis of Ag nanoparticles using Caralluma acutangula extract and its catalytic functionality towards degradation of hazardous dye pollutants. *Crystals* **2022**, *12*, 1069.

(51) Kassem, A. A.; Abdelhamid, H. N.; Fouad, D. M.; Ibrahim, S. A. Hydrogenation reduction of dyes using metal-organic framework-derived CuO@C. *Microporous Mesoporous Mater.* **2020**, *305*, 110340.

(52) Banazadeh, A.; Salimi, H.; Khaleghi, M.; Shafiei-Haghighi, S. Highly efficient degradation of hazardous dyes in aqueous phase by supported palladium nanocatalyst-a green approach. *J. Environ. Chem. Eng.* **2016**, *4*, 2178−2186.

(53) Malik, M. A.; Alshehri, A. A.; Abomuti, M. A.; Danish, E. Y.; Patel, R. Bioengineered Matricaria recutita extract-assisted palladium nanoparticles for the Congo red dye degradation and catalytic reduction of 4-nitrophenol to 4-aminophenol. *Toxics* **2021**, *9*, 103.

(54) Joseph, A.; Vellayan, K.; González, B.; Vicente, M. A.; Gil, A. Effective degradation of methylene blue in aqueous solution using Pd-supported Cu-doped Ti-pillared montmorillonite catalyst. *Appl. Clay Sci.* **2019**, *168*, 7−10.

(55) Najem, M.; Nada, A. A.; Weber, M.; Sayegh, S.; Razzouk, A.; Salameh, C.; Eid, C.; Bechelany, M. Palladium/carbon nanofibers by combining atomic layer deposition and electrospinning for organic pollutant degradation. *Materials* **2020**, *13*, 1947.

(56) El-Subruiti, G. M.; Eltaweil, A. S.; Sallam, S. A. Synthesis of active MFe2O4/γ-Fe2O3 nanocomposites (metal= Ni or Co) for reduction of nitro-containing pollutants and methyl orange degradation. *Nano* **2019**, *14*, 1950125.

(57) Subhan, F.; Aslam, S.; Yan, Z.; Yaseen, M.; Khan, K. A. Palladium nanoparticles decorated on ZSM-5 derived micro-/mesostructures (MMZ) for nitrophenol reduction and MB degradation in water. *J. Environ. Chem. Eng.* **2021**, *9*, 105002.

(58) Chhabra, T.; Kumar, A.; Bahuguna, A.; Krishnan, V. Reduced graphene oxide supported MnO_2 nanorods as recyclable and efficient adsorptive photocatalysts for pollutants removal. *Vacuum* **2019**, *160*, 333−346.

(59) Pujar, M. S.; Hunagund, S. M.; Khanapure, S.; Vootla, S. K.; Sidarai, A. H. Multifunctional ZnO/CeO_2 nanocomposites for Photoinduced dye degradation and Antibacterial activities. *J. Sol. Gel Sci. Technol.* **2022**, *101*, 356−369.

(60) Luo, F.; Yang, D.; Chen, Z.; Megharaj, M.; Naidu, R. One-step green synthesis of bimetallic Fe/Pd nanoparticles used to degrade Orange II. *J. Hazard. Mater.* **2016**, *303*, 145−153.